REGULAR ARTICLE

blood advances

# The role of miR-150-5p/E2F3/survivin axis in the pathogenesis of plasmablastic lymphoma and its therapeutic potential

Miriam Verdú-Bou,[1,2] Maria Joao Baptista,[2] Marcelo Lima Ribeiro,[3] Aleix Méndez-López,[4] Núria Profitós-Pelejà,[3] Fabian Frontzek,[5,6] Gaël Roué,[3] José Luís Mate,[7] Mireia Pellicer,[3] Pau Abrisqueta,[8] Josep Castellví,[9] Mariana Bastos-Oreiro,[10] Javier Menárguez,[11] Miguel Alcoceba,[12] Eva González-Barca,[13] Fina Climent,[14] Antonio Salar,[15] Juan-Manuel Sancho,[2,4] Annette M. Staiger,[16] German Ott,[16] Ioannis Anagnostopoulos,[17] Manel Esteller,[18] Georg Lenz,[5] Gustavo Tapia,[7,*] and José-Tomás Navarro[1,2,4,*]

[1]Department of Medicine, Universitat Autònoma de Barcelona, Badalona, Spain; [2]Lymphoid Neoplasms Group and [3]Lymphoma Translational Group, Josep Carreras Leukaemia Research Institute, Badalona, Spain; [4]Department of Hematology, Institut Catala d'Oncologia–Germans Trias i Pujol University Hospital, Badalona, Spain; [5]Department of Medicine A, Hematology, Oncology, and Pneumology, University Hospital Münster, Münster, Germany; [6]Centre for Lymphoid Cancer, BC Cancer, Vancouver, BC, Canada; [7]Department of Pathology, Germans Trias i Pujol University Hospital, Autonomous University of Barcelona, Badalona, Spain; [8]Department of Hematology and [9]Department of Pathology, Vall d'Hebron University Hospital, Barcelona, Spain; [10]Department of Hematology and [11]Department of Pathology, Gregorio Marañón Hospital, Madrid, Spain; [12]Department of Hematology, University Hospital of Salamanca (HUS/IBSAL), CIBERONC, Cancer Research Institute of Salamanca–IBMCC (USAL-CSIC), Salamanca, Spain; [13]Department of Hematology, Institut Catala d'Oncologia-Duran i Reynals Hospital, Bellvitge Biomedical Research Institute, University of Barcelona, Hospitalet de Llobregat, Spain; [14]Department of Pathology, Bellvitge University Hospital-IDIBELL, Hospitalet de Llobregat, Barcelona, Spain; [15]Department of Hematology, Hospital del Mar, Barcelona, Spain; [16]Department of Clinical Pathology, Robert Bosch Hospital, Stuttgart, Germany; [17]Department of Pathology, Institute of Pathology, University of Würzburg, Würzburg, Germany; and [18]Cancer Epigenetics Group, Josep Carreras Leukemia Research Institute and CIBERONC, Badalona, Spain

**Key Points**

- miR-150-5p acts as tumor suppressor by repressing the lymphomagenic-driver *E2F3*, leading to cell cycle disruption in PBL.
- E2F3 and survivin could serve as promising therapeutic targets for the management of PBL.

Plasmablastic lymphoma (PBL) is an uncommon and aggressive B-cell lymphoma with a poor prognosis. Some studies have described genetic alterations in PBL, but its transcriptome has been scarcely studied, and molecular mechanisms driving lymphomagenesis remain poorly understood. Our goal was to delineate transcriptomic profiles to identify potential biomarkers for novel targeted therapy in PBL. RNA sequencing uncovered an enrichment of cell cycle–related genes, including MYC and E2F targets, and genes involved in G2/M checkpoint in PBL. Microarray analyses discovered 2 microRNA expression signatures depending on the presence of *MYC* translocation. Interestingly, miR-150-5p was downregulated, whereas *E2F3* and *BIRC5* (survivin), a cell cycle activator and an antiapoptotic regulator, respectively, were upregulated. Increasing miR-150-5p in PBL-1 cells induced G1 cell cycle arrest, suppressed proliferation by transcriptionally repressing *E2F3*, and promoted apoptosis by the downregulation of *BIRC5*. Interestingly, the miR-150-5p tumor suppressor activity was diminished in *E2F3*-knockdown cells. The combined inhibition of E2F3 and survivin attenuated lymphomagenesis in PBL cells and suppressed tumor growth in a chorioallantoic membrane–derived xenograft model of PBL. Overall, our study highlights the pivotal role of the miR-150-5p/E2F3/survivin axis in boosting PBL lymphomagenesis and unveils new therapeutic targets for this lymphoma.



Submitted 10 February 2025; accepted 23 March 2025; prepublished online on *Blood Advances* First Edition 9 April 2025; final version published online 12 June 2025. https://doi.org/10.1182/bloodadvances.2025016180.

*G.T.G. and J.-T.N. contributed equally as senior authors to this study.

Microarray data have been deposited in the Gene Expression Omnibus (accession number GSE261612); RNA sequencing data have been deposited in the Sequence Read Archive (accession number PRJNA1090853).

The full-text version of this article contains a data supplement.

## Introduction

Plasmablastic lymphoma (PBL) is an uncommon B-cell lymphoma, more frequent among men with immunodeficiency and commonly associated with HIV infection.[1] Furthermore, 50% of patients harbor an *MYC* translocation (*MYC*-t) that results in a negative prognostic impact in these patients,[2,3] and 70% present Epstein-Barr virus (EBV) infection in the tumor cells.[4] This lymphoma mainly affects the oral cavity and gastrointestinal tract and has an aggressive clinical behavior.[4] The standard chemotherapy regimens used for PBL treatment exhibit limited efficacy in most patients, and these patients have a poor prognosis.[5]

Recently, some studies have shed light on the PBL genetic landscape. In particular, the JAK-STAT and RAS-MAPK have surfaced as central mutated signaling pathways, including *TP53*, *MYC*, *NRAS*, and *SOCS1* as the main mutated genes.[6-9] The occurrence of these mutations seems to be influenced by the presence of EBV and HIV infections in these patients.[6-9] In addition, the transcriptomic profile of PBL, explored in small cohorts, also seems to differ depending on EBV infection status. Ramis-Zaldivar et al described an attenuated expression of p53 signaling pathway–related genes and a tendency toward a decreased expression of genes in the NF-κB pathway in EBV-negative patients.[7] EBV infection also affects PI3K/Akt/mTOR signaling pathway, the major histocompatibility class I antigen presentation pathway, and cell cycle regulation.[8] In contrast, PBL exhibits variations in microRNA (miRNA) expression depending on the presence of HIV infection, although the miRNome of PBL remains practically unexplored.[10]

Although different studies have delineated the genetic landscape and transcriptome signatures, the molecular mechanisms of PBL lymphomagenesis remain incompletely elucidated. Understanding these mechanisms is imperative for identifying biomarkers for new therapeutic approaches. In this study, we disclosed the miRNA expression profile of PBL, revealing a downregulation of miR-150-5p, a miRNA with opposite roles in different cancers.[11] We demonstrated that this miRNA plays a tumor suppressor role in PBL by repressing the cell cycle regulators *E2F3* and *BIRC5* (survivin), which are upregulated in this lymphoma. In addition, our gene expression analysis uncovered an enrichment of cell cycle–associated genes, particularly E2F transcription factors, which are linked to increased proliferation in PBL. These findings support the notion that E2F family members and survivin represent bona fide therapeutic targets, as has been described in other cancer types.[12,13] Our in vitro and in vivo investigations point out that E2F3 and survivin may represent a new promising venue for PBL treatment.

## Methods

### Patients' samples

Formalin-fixed, paraffin-embedded samples of 66 PBL patients and 14 reactive lymph nodes (included as a control group) were included in the study (supplemental Methods).

### RNA-seq

For the gene expression study, RNA sequencing (RNA-seq) was performed using 2 μg of total RNA from formalin-fixed, paraffin-embedded samples. A total of 41 PBL and 14 control samples were sequenced in a paired-end run (2 × 150 bp) on the NovaSeq 6000 S4. Approximately 80 million paired-end reads were obtained per sample (supplemental Methods).

### Microarrays

For miRNA expression studies, 560 ng of total RNA from 66 PBL and 14 control samples were analyzed using the GeneChip miRNA 4.0 Array from Affymetrix (Thermo Fisher Scientific, Waltham, MA; supplemental Methods).

### CAM assay

The chorioallantoic membrane (CAM) assay was used as an in vivo model to evaluate the involvement of E2F3 in tumor proliferation and the effect of inhibitors HLM006474 (H) and S12 (S) on tumors formed by PBL-1 wild-type (WT) and *E2F3*$^{mut}$ cells. Hematoxylin-eosin staining and immunohistochemistry studies were performed in tumor samples (supplemental Methods).

All preclinical studies are detailed in supplemental Methods.

## Results

### Clinical features of the PBL cohort

The main clinical characteristics of the patients are shown in supplemental Table 1. Among patients with clinical data information, a higher percentage of HIV-negative patients was found (63% negative vs 37% positive), approximately half of PBL patients were EBV positive (42% negative vs 58% positive), and a similar proportion was observed for *MYC*-t (52% negative vs 48% positive). International Prognostic Index score (IPI) of intermediate/high was more frequent than IPI low among patients positive for these 3 variables, reaching statistical significance in individuals with HIV ($P = .001$; 83% IPI intermediate/high vs 17% IPI low).

### E2F-mediated cell cycle disruption in PBL

To further explore the transcriptomic landscape of PBL, we conducted RNA-seq analysis. Principal component analysis delineated distinct clustering between PBL and control samples, exhibiting greater dispersion among PBL patients (supplemental Figure 1A), indicating the heterogeneity within PBL. Differential expression analysis identified 1619 upregulated and 1337 downregulated coding genes between PBL and control groups ($\log_2$ fold change $>|1|$; adjusted $P < .05$; Figure 1A; supplemental Data 1). Functional enrichment analysis revealed an induction of cell cycle genes associated with the upregulation of MYC targets, E2F targets, and G2M checkpoint genes, as well as higher metabolic demands, encompassing glycolysis, cellular respiration, oxidative phosphorylation, and the mTORC pathway. These hallmarks were enriched in both EBV- and *MYC*-t–positive and –negative patients, compared independently to controls (Figure 1B; supplemental Data 2). Interestingly, when PBL patients were compared with controls based on the presence of EBV and *MYC*-t, an enrichment of genes involved in epithelial-mesenchymal transition was identified. On the contrary, PBL exhibited a downregulation of immune response activation (Figure 1C), with immune evasion mechanisms seemingly independent of EBV and HIV infection (supplemental Figure 1B; supplemental Data 2). After these results, we predicted the infiltration of immune cells in the tumor using the immune

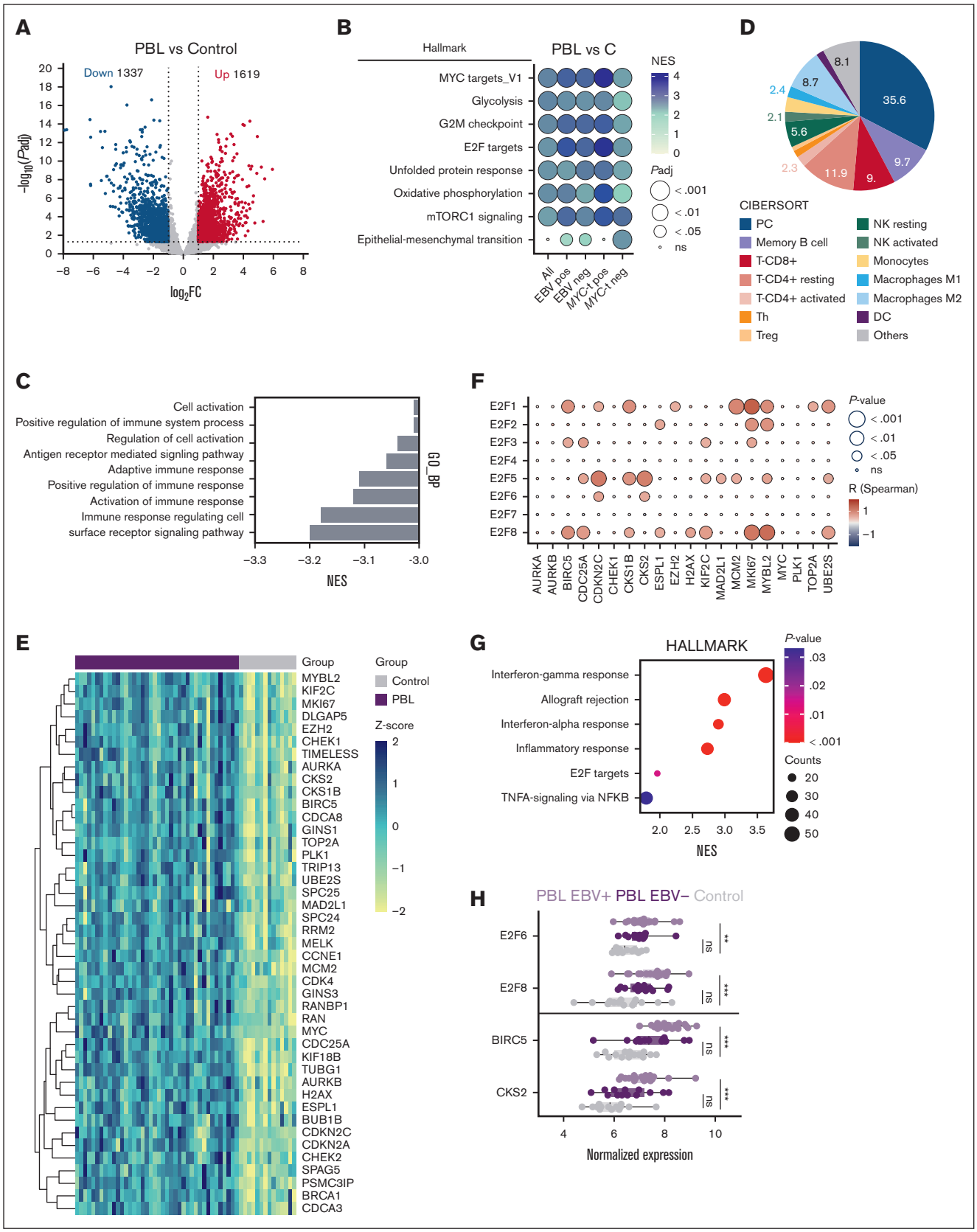


**Figure 1. MYC, E2F targets, and cell cycle–related gene upregulation in PBL.** (A) Volcano plot showing differentially expressed genes in PBL vs control ($log_2$ fold change [$log_2$FC] > |1|; adjusted *P* [*P*.adj] < .05), with significantly upregulated genes highlighted in red (1619 genes) and downregulated genes in blue (1337 genes). $Log_2$FC is depicted

cell deconvolution method CIBERSORT. This analysis revealed lower infiltration of activated $CD4^+$ T cells and natural killer cells than resting ones and more protumorogenic M2 macrophages than proinflammatory M1 macrophages in PBL tumors (Figure 1D).

Members of the E2F family (E2F1-8) are pointed as pivotal regulators of the cell cycle.[13] All members, except *E2F5,* exhibited upregulation in PBL (supplemental Figure 2A). The relevance of E2F members, particularly E2F1 and E2F4, and MYC as regulators of gene expression in PBL was disclosed through gene set enrichment analysis of transcription factor targets (supplemental Figure 2B). E2Fs are activated after the phosphorylation and inactivation of retinoblastoma and alteration in that mechanism has been associated with the development of several cancers.[13,14] Nevertheless, only lower *E2F1* levels, but not the rest of *E2F* genes, were associated with high *RB1* expression. These results suggest that *RB1* infraexpression is probably not the cause of the potentiation of the *E2F* family in PBL (supplemental Figure 2C).

Among E2F targets upregulated in PBL, most of them play critical roles in cell cycle progression, including G1/S transition (*CDC25A*, *CCNE1*, *MYC*, *RRM2*, and *CDK4*) and G2/M phases (*BIRC5*, *AURKB*, *CDCA8*, and *EZH2*; Figure 1E). Furthermore, 20 E2F targets overlapped with genes associated with the G2M checkpoint (recorded in both hallmark and gene ontology databases), including *BIRC5*, *CDC25A*, *CKS1B*, *MK67*, and *MYBL2*. A correlation analysis between the expressions of these 20 genes and *E2F1-8* revealed a positive association between *E2F1-3* and *E2F8* and the proliferation marker *MKI67* (Ki67; Figure 1F).

Moreover, we evaluated the impact of EBV presence in tumoral cells in the disruption of gene expression. In this regard, EBV-positive PBL also exhibited an enrichment of E2F targets compared with EBV-negative PBL and a significant overexpression of *E2F6* and *E2F8,* as well as the E2F targets *BIRC5* and *CKS2*, compared with controls (Figure 1G-H).

Altogether, our data suggest that E2Fs may represent new lymphomagenic drivers in PBL, resulting in uncontrolled cell cycle progression and abnormal proliferation, and EBV could be involved in E2F targets abnormal expression.

## miRNA expression profile in PBL

***miRNA expression pattern is associated with* MYC-t.** To gain deeper insight into the transcriptome of PBL, we performed a miRNA array study. We identified 56 differentially expressed miRNAs (DEMs), with miR-148a-3p and miR-4417 being the most upregulated and miR-150-5p, miR-342-5p, miR-342-3p, miR-1972, and miR-3609 the most downregulated (Figure 2A; supplemental Data 3). Considering the 36 DEMs with validated targets according to Affymetrix annotations, we distinguished 3 clusters: 1 control-associated (C3) and 2 PBL-associated clusters (C1 and C2), pointing to a heterogeneity among PBLs regarding miRNA expression (Figure 2B). Interestingly, C1 was significantly associated with *MYC*-t (58% *MYC*-t positive vs 42% *MYC*-t negative) compared to C2 (33% *MYC*-t positive vs 67% *MYC*-t negative; $P = .0006$; Figure 2C). The increased messenger RNA (mRNA) levels of *MYC* due to *MYC*-t (supplemental Figure 3A) could orchestrate an alteration of the miRNA expression pattern in PBL. We also examined the expression of the miR-17-92 cluster, which is activated by c-Myc and functions as one of the well-described pathogenic mechanisms associated with this oncoprotein.[15,16] However, no significant changes in miR-17-92 cluster expression were detected in this lymphoma compared to controls (supplemental Data 3), nor between *MYC*-t–positive and *MYC*-t–negative PBL (data not shown).

***miRNAs regulate cell cycle control and tumor progression–associated pathways.*** To understand how these miRNAs may disrupt cellular processes in PBL, we conducted an enrichment analysis of the validated targets of DEMs. Consistent with the findings in gene expression analysis, these miRNAs regulate MYC and E2F targets, as well as genes involved in G2/M checkpoint (Figure 2D). Additionally, these miRNAs are implicated in oncogenic mechanisms, including apoptosis and signaling pathways involved in proliferation, such as NF-κB and PI3K-Akt-mTOR.

Given the cell cycle disruption observed in PBL according to both transcriptomic analyses, we focused on interactions between miRNAs and their overexpressed targets in PBL involved in cell cycle–related enriched hallmark data sets (Figure 2E-F). Specifically, miR-148a-3p and miR-150-5p mainly regulate E2F targets and G2/M-associated genes, including *MYC*, *AURKB*, and *CCNA2* (regulated by miR-148a-3p), as well as *BIRC5*, *CCNE1*, and *EZH2* (regulated by miR-150-5p). On the contrary, *MYB* is a well-established target of miR-150-5p, as documented in previous studies,[17-19] and it plays a role in G2/M cell cycle progression.[20] Although a prior cohort reported enrichment of MYB targets in PBL,[21] our analysis revealed no overexpression of *MYB* compared with controls (supplemental Data 1) and no negative correlation between miR-150-5p and *MYB* expression (supplemental Figure 3B). We used predictive tools such as miRDB, miRmap, and TargetScan to identify additional potential targets of the most DEMs. Notably, *E2F3* was predicted to be a target of the most downregulated miRNA, miR-150-5p, an interaction previously

**Figure 1 (continued)** in the x-axis and $\log_{10}$(*P*adj) in the y-axis. (B) GSEA of hallmark data set for upregulated genes in PBL. The figure includes different comparisons between PBL and controls depending on the presence of EBV and *MYC*-t in tumoral cells. Both, NES and *P*adj are represented by color and symbol size, respectively. (C) GO analysis for downregulated genes in PBL. The figure shows NES (x-axis) and the gene sets with *P*adj <.0001 (y-axis). (D) Infiltrating immune cells (%) in PBL according to CIBERSORT immune deconvolution analysis. (E) Heat map displaying the expression of upregulated E2F targets in PBL, involved in the cell cycle. PBL and controls (top) are identified in purple and pink, respectively. The color of the heatmap is represented by the z-score. (F) Correlation between the expression of *E2F* and their 20 targets associated with G2M checkpoint in PBL patients according to hallmark and GO data sets. *R* value is represented with color heatmap and *P* value by circle size. (G) GSEA based on hallmark gene set in EBV-positive vs EBV-negative PBL including all coding genes. *P* value and gene counts are represented by color and symbol size, respectively. (H) Differential expression of the *E2F* members (top) and the E2F targets *BIRC5* and *CSKS2* (bottom) depending on EBV infection. Statistical analysis was performed using Spearman test for correlation analysis in panel F; Dunn multiple comparisons test in panel H; **P* < .05; ***P* < .01; ****P* < .001. DC, dendritic cell; GO, gene ontology; GSEA, gene set enrichment analysis; NES, normalized enrichment score; NK, natural killer; ns, not significant; PC, plasma cell; Th, T-helper; TNFA, tumor necrosis factor alpha; Treg, regulatory T cell.

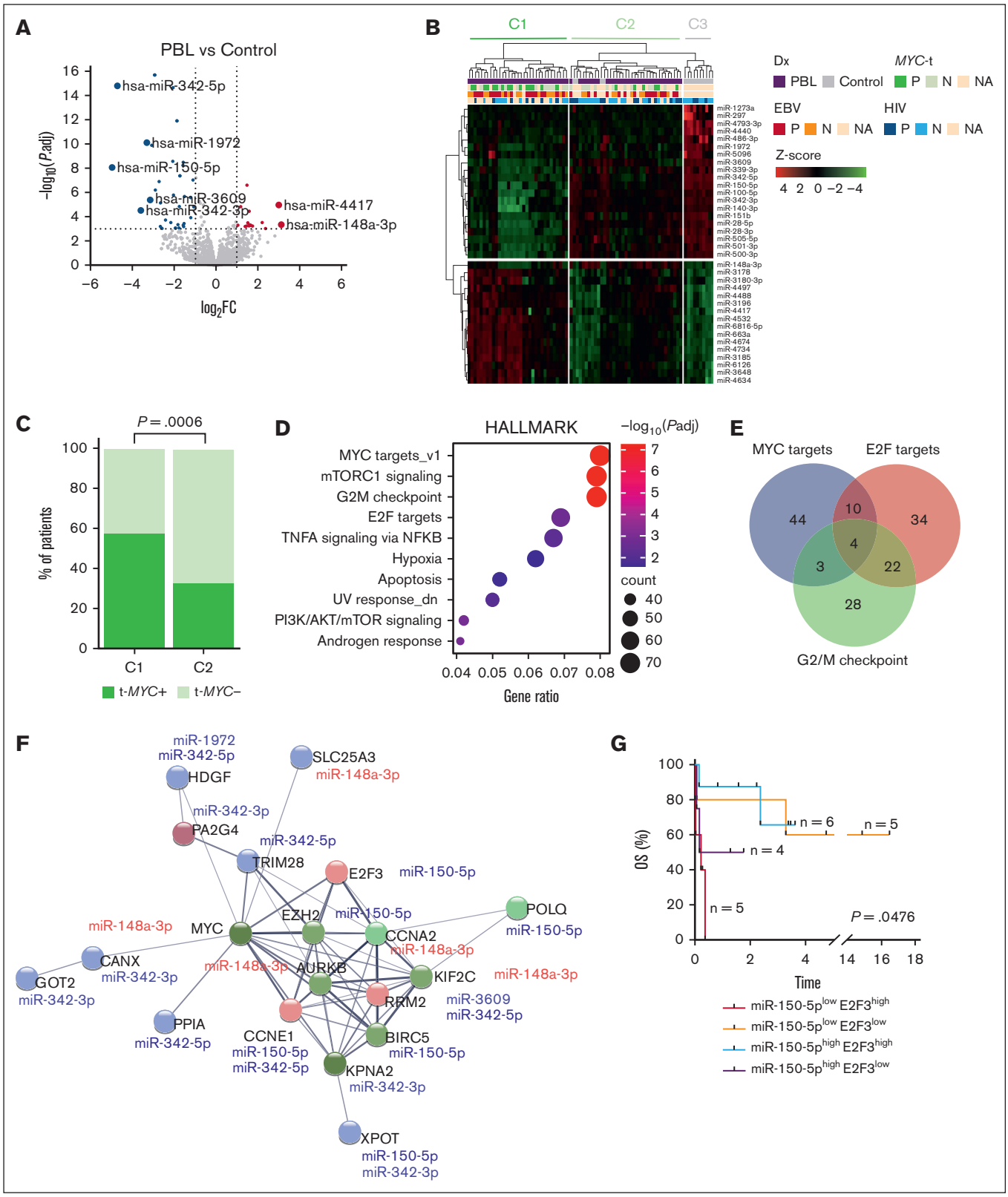


**Figure 2. miRNA landscape in PBL.** (A) Volcano plot highlighting DEMs in PBL compared to controls, with significantly upregulated genes (red) and downregulated genes (blue; $\log_2FC > |1|$; $P$adj $< .001$). (B) Heatmap displaying unsupervised analysis between PBL (purple) and controls (gray) of 36 DEMs with validated targets based on Affymetrix annotations ($\log_2FC > |1|$; $P$adj $< .001$). On top, patients are classified depending on Dx, HIV and EBV infections, and *MYC*-t. The color of the heat map is represented by the z-score. Three clusters are highlighted on top, PBL-associated clusters (C1 and C2; green) and control-associated cluster (C3; gray). (C) This figure exhibits the proportion of

demonstrated by Meng et al.[22] Analyzing the prognostic impact of miRNA targets in PBL, we found that patients with low miR-150-5p and high *E2F3* expressions exhibited the poorest overall survival, with a median survival of 0.2 years ($P = .0486$; Figure 2G).

## miR-150-5p acts as a tumor suppressor in PBL

Given the downregulation of miR-150-5p, the relevance of E2F as gene expression regulators, and the prognostic impact of miR-150-5p/*E2F3* expression in PBL, we focused on investigating the role of this interaction in PBL lymphomagenesis. Firstly, we hypothesized that miR-150-5p could act as a tumor suppressor miRNA in this disease. To address this goal, we analyzed miR-150-5p correlation with its validated target genes and with proliferation. A significant negative correlation was found between miR-150-5p and *E2F3* ($P = 2.32 \times 10^{-6}$) and *BIRC5* ($P = 4.87 \times 10^{-8}$). *BIRC5* is transcriptionally activated by E2F3[23]; hence, we observed a positive correlation between *E2F3* and *BIRC5* ($P = 1.17 \times 10^{-6}$) in PBL (Figure 3A). Expression of both genes positively correlated with the proliferation marker *MKI67,* in an opposite manner to that of miR-150-5p (supplemental Figure 4B). The miR-150-5p/*E2F3*/*BIRC5* axis expression was validated at mRNA and protein levels by quantitative reverse transcription polymerase chain reaction and immunohistochemistry, respectively (supplemental Figure 4B-D).

Next, we conducted miR-150-5p overexpression experiments by transfecting PBL-1 cells with miR-150-5p mimics (supplemental Figure 5A). The overexpression of miR-150-5p elicited significant repression of *E2F3* and *BIRC5* (survivin) transcription (Figure 3B), leading to a 37% and 39% decrease in their protein levels, respectively (Figure 3C). To validate the union of miR-150-5p with the *BIRC5* 3′ untranslated region, we conducted a luciferase assay in HEK-293T cells, demonstrating a significant 20% reduction in luciferase activity (Figure 3D; supplemental Figure 5). Although we confirmed that miR-150-5p can bind to the *BIRC5* 3′untranslated region, it does not seem to strongly repress this gene. Moreover, survivin is activated by Aurora B (*AURKB*), another overexpressed gene in PBL. Both proteins are components of the chromosomal passenger complex, which is essential for ensuring the chromosomal segregation during mitosis.[24] miR-150-5p overexpression did not change Aurora B mRNA or protein levels but impaired its activation by decreasing the phosphorylated state (Figure 3B-C). These results suggest that miR-150-5p may also contribute indirectly to the inactivation of its protein. Additionally, we analyzed whether *STAT3*, a mutated gene in PBL and a regulator of *BIRC5,* could be responsible for *BIRC5* overexpression. Nevertheless, no positive correlation between the expression of both genes was detected in PBL patients (supplemental Figure 3B). The cells overexpressing miR-150-5p showed reduced viability and increased apoptosis rates compared to those transfected with negative control miRNA (Figure 3E). In addition, miR-150-5p deregulated the cell cycle, leading to an arrest at the G1 phase in PBL-1 after 24 hours (Figure 3F). Consequently, there was a 20% reduction in cell proliferation at 72 hours after transfection (Figure 3G). These findings collectively suggest that miR-150-5p could prevent tumor progression by repressing *E2F3* and *BIRC5*, thereby promoting apoptosis and preventing cell cycle progression.

## E2F3 drives lymphomagenesis in PBL

After the previous results, we next explored the involvement of E2F3 in the pathogenesis of PBL. To address this goal, *E2F3* mutants ($E2F3^{mut1}$ and $E2F3^{mut2}$) in the DNA binding domain (supplemental Figure 6; supplemental Methods) were generated in PBL-1 cells by CRISPR-Cas9 editing tool. Both $E2F3^{mut1}$ and $E2F3^{mut2}$ resulted in *E2F3* knockdown cell lines (Figure 4A-C). Exploring cell cycle–related gene expression revealed significantly reduced mRNA and protein levels of *BIRC5*/survivin, cyclin A2, and Aurora B in the 2 $E2F3^{mut}$ cell lines compared with PBL-1 WT cells (Figure 4A-C). To a lesser extent, decreased expression of EZH2, RRM2, and cyclin E1 was detected. Moreover, both *E2F3* mutant cell lines displayed significant G1 phase arrest and proliferation inhibition (Figure 4D,F). Next, we assessed the implication of E2F3 in the migratory and invasive capabilities of PBL-1 cells. Both $E2F3^{mut1}$ and $E2F3^{mut2}$ cells exhibited a substantial loss of invasive potential (80% and 63%, respectively) and a moderate decline in migratory capacity (34% and 58%, respectively; Figure 4E).

To confirm the role of E2F3 in tumor proliferation, 2 chicken CAM-derived PBL models, by engrafting both PBL-1 WT and $E2F3^{mut}$ cells (clone 1) were generated (supplemental Methods). The tumors formed by $E2F3^{mut}$ cells showed a remarkable reduction in PBL $CD138^{+}$ cells (Figure 4G), along with an 87% reduction in their proliferative capacity (Figure 4H). These findings support our earlier in vitro findings that suppressing *E2F3* attenuates PBL-1 cell proliferation.

## miR-150-5p/E2F3–negative regulatory loop

Considering the negative correlation between miR-150-5p and *E2F3,* we next investigated whether E2F3 might also regulate miR-150-5p in a negative regulatory loop. The precursor miR-150 is repressed by MYC,[25] which is transcriptionally activated by E2F3. Indeed, the expression of miR-150-5p was associated with an increased *MYC* expression, including controls and PBL samples, but miR-150-5p was not overexpressed in PBL *MYC*-t–positive patients compared with negative ones (supplemental Figure 3B-C). To address whether E2F3 and MYC cooperate to downregulate the tumor suppressor miR-150-5p, we also generated a *MYC* knockout ($MYC^{KO}$) in PBL-1 cells using

**Figure 2 (continued)** patients in clusters C1 and C2, depending on *MYC*-t. (D) Enrichment analysis of miRNA targets that were differentially expressed ($\log_2FC > |1|$; $Padj < .001$) based on hallmark gene sets. Bubble color and size represent $-\log_{10}(Padj)$ and gene count, respectively. (E) Venn diagram illustrating the number of overlapping enriched gens between G2/M checkpoint (green), MYC targets (blue), and E2F targets (pink) hallmark data sets. (F) miRNA target network performed with STRING (version 12.0) including the most DEMs ($\log_2FC > |3|$; $Padj < .001$) and their validated targets according to Affymetrix annotations (represented in circles; $\log_2FC > |1|$; $Padj < .05$). The colors of the circles represent the hallmark data sets in which each gene is involved, according to the colors of the Venn diagram in panel E. The color of miRNAs represents the downregulation (blue) or upregulation (red). (G) OS of PBL depending on miR-150-5p and *E2F3* expression (median normalized expressions, 6.50 and 8.43, respectively). Statistical analysis was performed using Fisher exact test in panel C and the log-rank test in panel G. Dx, diagnosis; N, negative; NA, not available; OS, overall survival; P, positive; TNFA, tumor necrosis factor alpha.

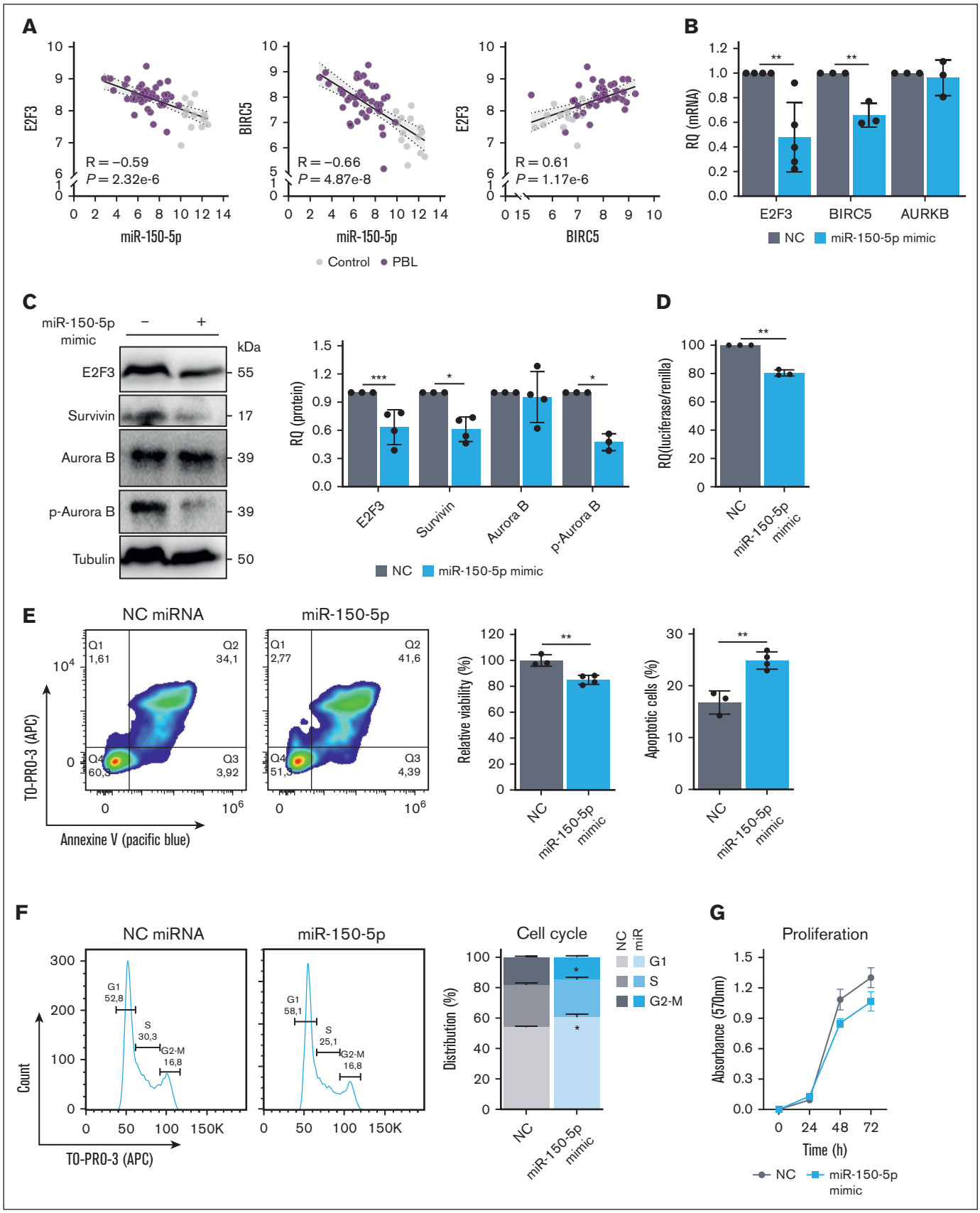


**Figure 3.**

CRISPR-Cas9 editing tool. We confirmed that E2F3 down-regulation leads to decreased c-Myc protein levels (Figure 4B-C), and the loss of *MYC* lead to reduced E2F3 ones (Figure 5A). Both $MYC^{KO}$ and $E2F3^{mut}$ cell lines harbored higher miR-150-5p levels than WT cells (Figure 5B). In addition, both $MYC^{KO}$ and $E2F3^{mut}$ reached higher miR-150-5p levels when cells were nucleofected with miR-150-5p mimic than WT cells (Figure 5C). These findings reinforce our hypothesis of a negative regulatory loop between *E2F3* and miR-150-5p mediated by c-Myc.

### E2F3 is an essential target of miR-150-5p in the regulation of the cell cycle and apoptosis

To elucidate the relationship between miR-150-5p and *E2F3* in the pathogenesis of PBL, we evaluated the effect of miR-150-5p overexpression in $E2F3^{mut}$. miR-150-5p overexpression in $E2F3^{mut}$ cells was associated with impaired proliferation (Figure 5D). However, it did not alter the cell cycle or trigger apoptosis when compared with negative control miRNA-treated group (Figure 5E-F) because no changes in *E2F3*, *BIRC5*, and *CCNE1* were induced in $E2F3^{mut}$ (Figure 5G-I). These results indicate that miR-150-5p reduces its role as a tumor suppressor under *E2F3*-reduced conditions, suggesting that *E2F3* might be a relevant miR-150-5p target in the regulation of cell cycle progression and apoptosis repression in PBL.

### E2F3 and survivin as potential therapeutic targets of PBL-1

Given the involvement of the miR-150-5p/E2F3/survivin axis in PBL malignancy, we assessed the potential of E2F3 and survivin as therapeutic targets. We selected the E2F family inhibitor H and the survivin dimerization inhibitor S and determined their 50% inhibitory concentration ($IC_{50}$) values in PBL-1 (H, 7 μM; S, 25 μM; supplemental Figure 7A). The 2 treatments and the combination decreased both E2F3 and survivin protein levels at their $IC_{50}$ doses, which was more accentuated with the combination treatment (Figure 6A; supplemental Figure 7B). Both H and S inhibitors, as monotherapy or in combination, reduced viability and induced apoptosis in a dose-dependent manner in PBL-1, with the combination therapy proving most effective (Figure 6B; supplemental Table 2).

Consistent with E2F and survivin roles as cell cycle regulators, H and S treatments led to an increased proportion of cells in the G1 (14%) and G2/M phases (16%) of the cell cycle, respectively (Figure 6C). The combination also induced cell cycle arrest in G2/M phases (18%). Consequently, a reduction of proliferation in a dose-dependent manner was observed with different treatments, reaching higher inhibition with the H + S combination than either treatment alone (Figure 6D).

To further validate the antitumoral effect of H + S combination in PBL, we tested it in diffuse large B-cell lymphoma (DLBCL) cell lines, a closely related entity to PBL. Firstly, we confirmed that DLBCL cell lines exhibited lower E2F3 protein levels than PBL-1 (supplemental Figure 7C). Consequently, treatment with the H + S inhibitor combination induced higher cytotoxicity at lower doses in PBL-1 than in DLBCL cells (supplemental Figure 7D).

To further assess the efficacy of these agents, we evaluated their antitumor properties in the previously described PBL-CAM model (Figure 6E). After 9 days of embryo development, PBL-1 cells were seeded onto the chicken membrane, compounds were administered topically at the $IC_{50}$ dose at days 12 and 14, and the tumors were harvested at day 16. Notably, the treatment with H + S combination significantly impaired tumor growth (Figure 6F). After our in vitro findings, both H and S treatments led to a reduced proliferation of PBL-1 cells in vivo (Figure 6G-J). Altogether, these data suggest that targeting E2F3 and survivin might represent a promising therapeutic approach for PBL treatment.

## Discussion

To our knowledge, this report constitutes the most extensive transcriptomic and preclinical investigation conducted in PBL so far. Using RNA-seq analyses, significant disruptions in the cell cycle genes were identified. In particular, the transcription factors MYC and E2F play a key role in gene expression regulation and cell cycle disruption in this lymphoma. Genetic alterations such as amplifications or deletions of E2F have been associated with cancer development and with shorter overall survival.[13,14,26-28] In PBL, the transcription factors *E2F* were enriched, with some associated with the potentiation of the proliferation marker *MKI67*. In addition, the negative prognostic impact of high *E2F3* and low miR-150-5p expressions evoke the potential role of E2F as lymphomagenic drivers of PBL for the first time.

Our analyses uncover an increased metabolic activity in PBL, characterized by enriched oxidative phosphorylation, which has been involved in chemotherapy resistance across various lymphoproliferative disorders.[29,30] Thus, targeting the mitochondrial oxidative phosphorylation system might be a potential therapeutic strategy for PBL treatment.[31,32] Lymphomas associated with HIV and EBV exhibit a more permissive microenvironment.[33-35] Nevertheless, we detect immune evasion in PBL, irrespective of EBV or

**Figure 3. Tumor suppressor role of miR-150-5p in PBL.** (A) Spearman correlation between the expression of miR-150-5p and its targets *BIRC5* and *E2F3*, as well as correlation between *E2F3* and *BIRC5* (E2F3 target). PBL and controls are represented in purple and gray, respectively. (B) Relative *E2F3*, *BIRC5*, and *AURKB* gene expression by reverse transcription polymerase chain reaction (RT-qPCR) at 72 hours. (C) E2F3, survivin, Aurora B, and p-Aurora B protein expression by western blot at 72 hours (left) and relative protein expression (right). (D) Relative luciferase activity (RQ) normalized to Renilla activity comparing HEK-293T cells transfected with miR-150-5p mimic or with NC miRNA and plasmid that contains luciferase gene followed by *BIRC5* 3′ untranslated region. (E) Flow cytometry plots (left) of apoptosis at 24 hours by annexin V (Pacific Blue)/TO-PRO-3 (APC) staining and flow cytometry; plots (right) of relative viability and percentage of apoptotic cells (early plus late) of cells nucleofected with miRNA NC and miR-150-5p mimic, normalized to PBL-1 nontreated cells. (F) Cell cycle at 24 hours by flow cytometry and staining with TO-PRO-3 and flow cytometry. The percentage of cells in each phase of the cell cycle is shown. (G) 3-(4,5-dimethylthiazol-2-yl)-2,5-diphenyltetrazolium bromide assay indicates cell proliferation of cells treated with NC miRNA or miR-150-5p mimic at 0 hour and after 24, 48, and 72 hours of treatment. All figures represent PBL-1 nucleofected with NC miRNA in gray and with miR-150-5p mimic in blue. The *t* test was used for statistical analysis; $*P < .05$; $**P < .01$; $***P < .001$. All experiments were performed in triplicates unless otherwise specified. NC, negative control; RQ, relative quantity.

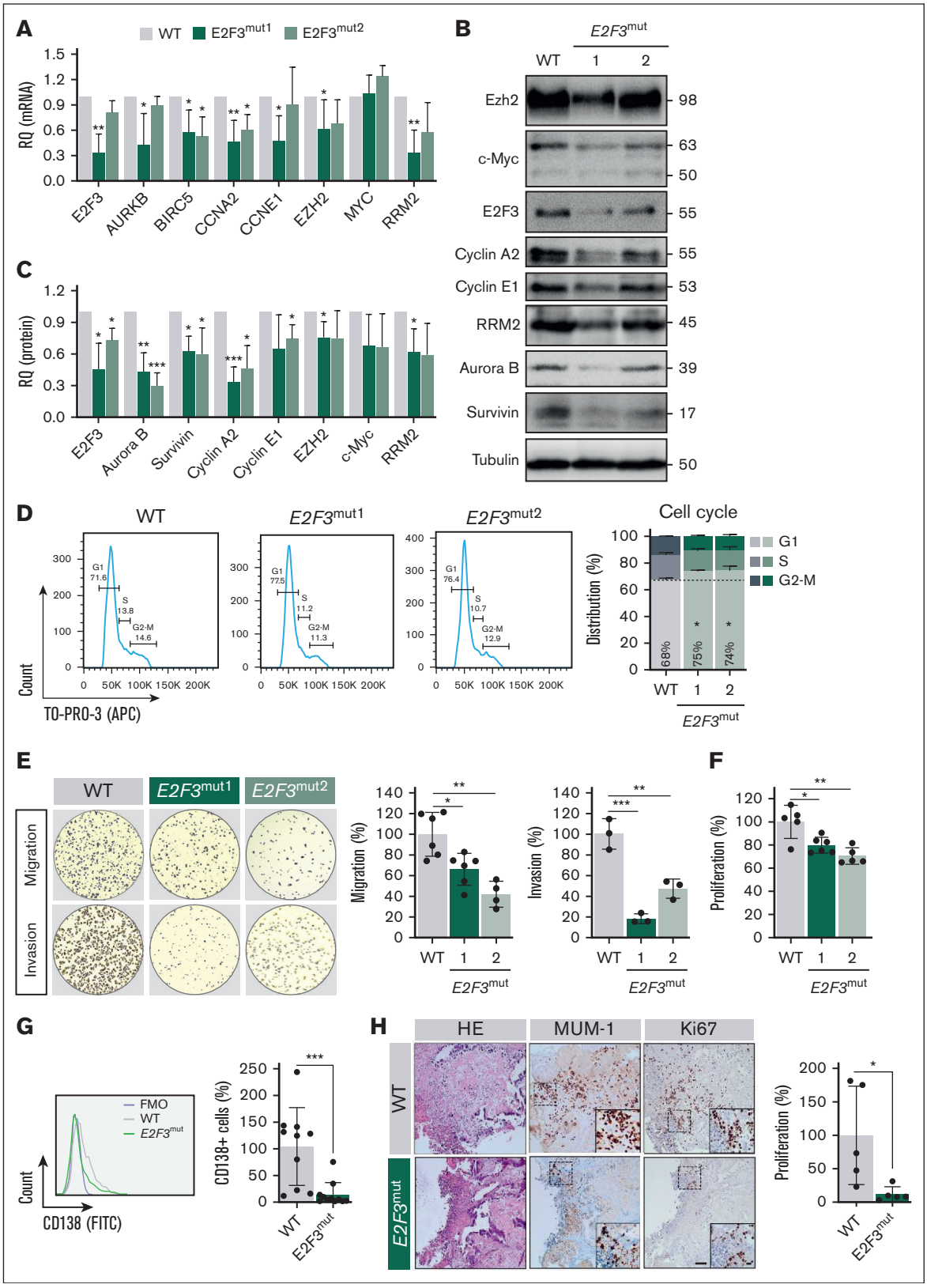


**Figure 4. E2F3 contributes to lymphomagenesis of PBL.** (A) Relative mRNA expression of *E2F3* and target genes involved in cell cycle, in PBL-1 *E2F3*$^{mut1}$ and *E2F3*$^{mut2}$ (green) normalized to WT cells (gray). (B) Representative western blot images of E2F3 and its targets involved in cell cycle, in PBL-1 WT, *E2F3*$^{mut1}$, and *E2F3*$^{mut2}$ cells. (C) The relative protein expression normalized to PBL-1 cells. (D) Cell cycle was assessed by flow cytometry through TO-PRO-3 (APC) staining (left), and the percentage of cells in each

HIV infections. These findings strengthen the notion that the tumor itself harbors gene signatures that enable evasion of immune recognition.

The functionality of miR-150-5p in cancer remains controversial. This miRNA has been characterized both as an onocmiR[36,37] and as a tumor suppressor miRNA in various cancers.[11,38,39] The in vitro overexpression of miR-150-5p in PBL-1 results in the repression of target genes such as *E2F3* and *BIRC5,* leading to programmed cell death, inhibition of proliferation, and cell cycle G1/S transition, confirming the tumor suppressor role of miR-150-5p in this lymphoma. Cell cycle arrest in G1 phase induced by the precursor miR-150 has also been described in follicular lymphoma.[25] miR-150-5p has been shown to impair the phosphorylation of Aurora B, an activator of survivin, both of which are part of the chromosomal passenger complex, essential for mitosis progression.[24] Our results point to miR-150-5p could prevent an uncontrolled mitosis by directly repressing *E2F3* and *BIRC5* and could partially impair survivin activation by avoiding Aurora B phosphorylation.

The MYC/miRNA network has been involved in cancer development, including different lymphomas.[40,41] Several miRNAs regulate *MYC* expression, whereas MYC, in turn, may repress tumor suppressor miRNAs or activate oncomiRNAs.[42,43] To our knowledge, this is the most comprehensive miRNA expression study, and it reveals that PBL exhibits different miRNA expression profiles depending on *MYC*-t. This finding suggests that the modulation of the miRNA landscape could be a mechanism of MYC-driven lymphomagenesis in PBL. In this study, we demonstrated that c-Myc induces miR-150-5p repression, as evidenced by increased miR-150-5p levels in $MYC^{KO}$ cells. In this sense, Myc impairs miR-150 maturation by activating *LIN28*, as described in acute myeloid leukaemia with MLL rearrangement.[17] However, in this PBL cohort, *LIN28A* showed no detectable expression (median count <5), suggesting that other c-Myc–activated mechanisms might be responsible for the underexpression of miR-150-5p in PBL.

Despite the upregulation of miR-150-5p in *E2F3* knockdown cells, no effects were observed on *E2F3*, *BIRC5*, and *CCNE1* expression, apoptosis, or cell cycle, suggesting that *E2F3* is essential for miR-150-5p's tumor suppressor role by controlling these cellular processes. Thus, the repression of *BIRC5* and *CCNE1* upon miR-150-5p upregulation may be indirectly mediated by E2F3 downregulation rather than a direct targeting by miR-150-5p. However, miR-150-5p can prevent proliferation independently of *E2F3* loss, probably by repressing other proliferation-related genes.

Considering previous discoveries, we hypothesized that E2F3 might play a significant role as a PBL-lymphomagenic driver. We demonstrate that *E2F3* knockdown leads to the repression of *CCNE1* and *CCNA2* transcription, both key regulators of G1/S transition, and a downregulation of *BIRC5*/survivin and *AURKB*, essential regulators of mitosis. It is worth noting that survivin is also relevant for G1/S transition in cell cycle progression, independent of mitogen signaling in B cells.[44] The Aurora B/survivin/mTOR axis has been linked to the G1-S transition in T cells.[45] These findings align with the increased percentage of cells in G1 phase in *E2F3* knockdown cells. Loss of E2F3 may trigger compensatory mechanisms that increase the levels of E2F1 and E2F2,[46] which would explain the lack of more pronounced accumulation of cells in G1 in *E2F3* knockdown cells. Moreover, reduced levels of E2F3 in PBL-1 exhibited limited migratory and invasive capacity in vitro and a decreased cell proliferation in vitro and in vivo. These findings collectively suggest that the suppression of E2F3 attenuates lymphoproliferative mechanisms in PBL-1, thereby reinforcing the notion that E2F3 is implicated in PBL malignancy.

High levels of survivin[47,48] and E2F[49] have been associated with poor prognosis in various cancers. Consequently, targeting survivin with the inhibitor S[50,51] and E2F with H[52,53] were proposed as potential therapeutic strategies in different cancers. Treatment of PBL-1 cells with these inhibitors results in cell cycle arrest and decreased proliferation. Although some studies have suggested that H inhibitor acts directly against E2F4 and increases E2F3 levels,[52,53] our results demonstrated a dose-dependent inhibition of E2F3 in PBL-1 cells. The combination of H and S inhibitors results in heightened sensitivity in PBL-1 cells. The G1 cell cycle arrest caused by the combination of inhibitors may result from the faster action of H than S or possibly because of increased disruption of the G1 phase transcriptional program. The synergy between the inhibitors likely comes from disrupting the transcription and activity of many genes controlling proliferation, cell cycle progression, and apoptosis, among others. These findings collectively indicate that targeting jointly E2F3 and survivin could be a promising therapeutic strategy for PBL treatment.

In conclusion, our comprehensive study provides new perspectives on the molecular pathogenesis of PBL, underscoring the tumor suppressor role of miR-150-5p and the dysregulation of cell cycle control orchestrated by E2Fs. Furthermore, our findings shed light on the involvement of the miR-150-5p/E2F3/survivin axis in tumor progression in PBL. Ultimately, targeting E2F and survivin may hold potential as a therapeutic strategy for PBL treatment.

**Figure 4 (continued)** cell cycle phases are shown in PBL-1 WT, $E2F3^{mut1}$, and $E2F3^{mut2}$ cells (right). (E) Migration and invasion of WT, $E2F3^{mut1}$, and $E2F3^{mut2}$ cells were determined at 48 hours in 5-µm-pore membranes of transwell inserts. The cells that migrated and invaded the lower chamber were fixed, stained with Giemsa, and counted (left). Relative migration and invasion plots (%) are shown (right). (F) Cell proliferation was determined by 3-(4,5-dimethylthiazol-2-yl)-2,5-diphenyltetrazolium bromide assay and relative proliferation of *E2F3* mutant cells normalized to WT ones is shown. (G) PBL-1 cells were inoculated in the chicken CAM in vivo model. The number of tumoral cells in the tumors developed after 7 days after cell inoculation was assessed by CD138-FITC staining. Flow cytometry plot of cells expressing CD138 (left) and the relative $CD138^{+}$ cells in $E2F3^{mut}$ tumors normalized to WT ones (right). (H) Representative images of hematoxilin-eosin (HE), MUM-1, and Ki67 immunohistochemistry staining from formalin-fixed, paraffin-embedded sections of CAM samples (left); and relative proliferation of WT and $E2F3^{mut}$ tumors (right). All in vitro experiments were performed in biological triplicates and technical duplicates unless otherwise specified; in vivo CAM experiments were performed in 5 to 10 eggs. Statistical significance was determined by *t* test or analysis of variance (ANOVA) test or *t* test. $^{*}P < .05$; $^{**}P < .01$; $^{***}P < .001$. FITC, fluorescein; HE, hematoxylin and eosin.

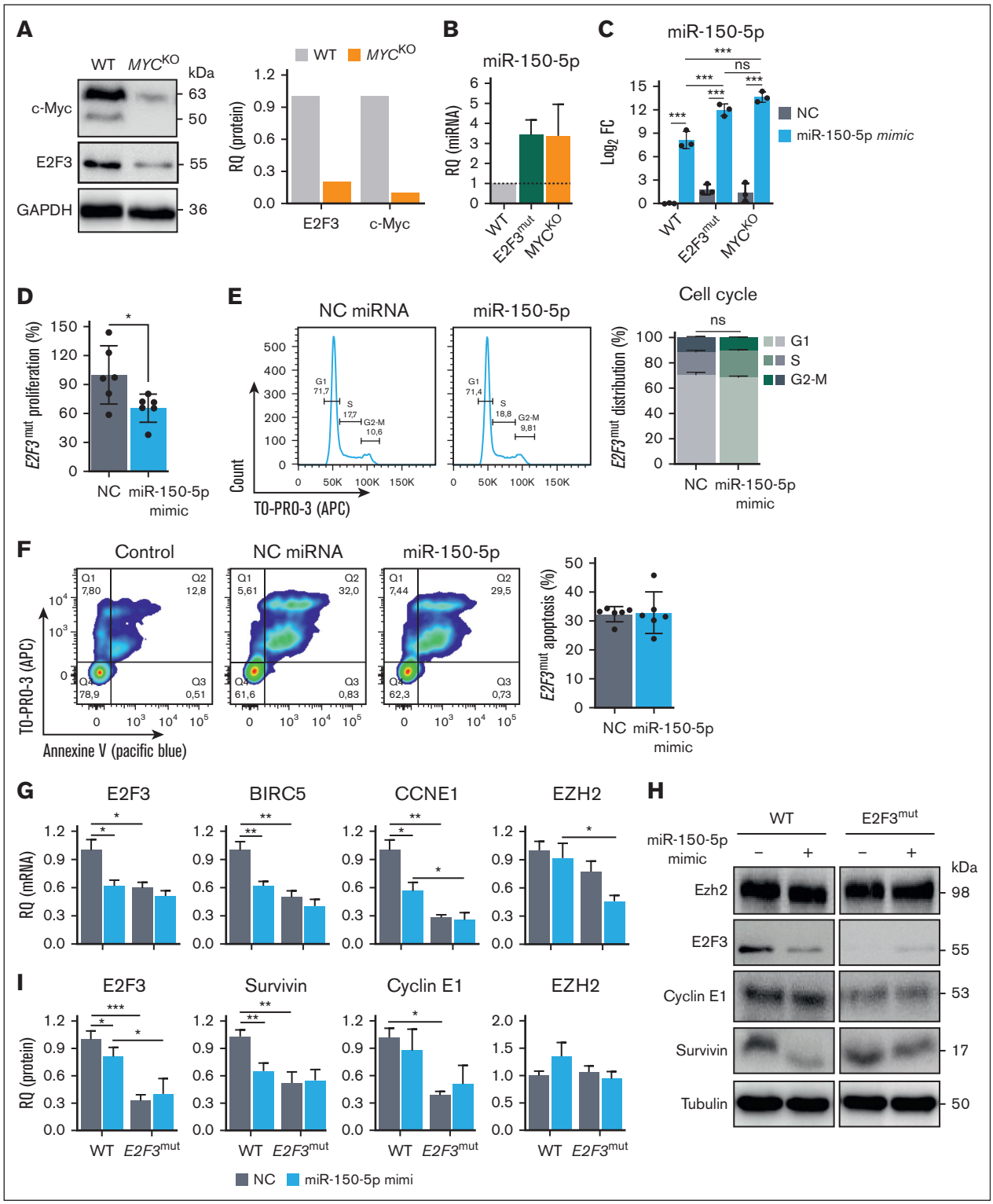


**Figure 5. The antitumoral effect of miR-150-5p is diminished in *E2F3*$^{mut}$ cells.** (A) Protein expression of E2F3, c-Myc, and in PBL-1 (WT; gray) and *MYC*$^{KO}$ (orange) cells showing the western blot plots (left) and relative expression (RQ; right) normalized to GAPDH. (B) Relative expression (RQ) of miR-150-5p in WT (gray), *E2F3*$^{mut}$ (green), or *MYC*$^{KO}$ (orange) cells. (C) Comparison of miR-150-5p expression when cells are transfected with NC miRNA (gray) or miR-150-5p mimic (blue) into WT, *E2F3*$^{mut}$, or *MYC*$^{KO}$ cells, measured by RT-qPCR. (D) Cell proliferation was evaluated by 3-(4,5-dimethylthiazol-2-yl)-2,5-diphenyltetrazolium bromide assays in NC miRNA and miR-150-5p mimic–transfected *E2F3*$^{mut}$ cells. (E) Cell cycle stages were assessed by flow cytometry with TO-PRO-3 staining and flow cytometry at 72 hours in *E2F3*$^{mut}$ cells transfected with NC miRNA or miR-150-5p mimic; figures show the percentage of cells in each stage. (F) Flow cytometry plots of apoptosis (left) evaluated by annexin V (Pacific Blue)/TO-PRO-3 (APC) staining 24 hours after transfection. Plots of relative viability of miR-150-5p transfected cells normalized to NC miRNA transfected ones; and percentage of apoptotic (early

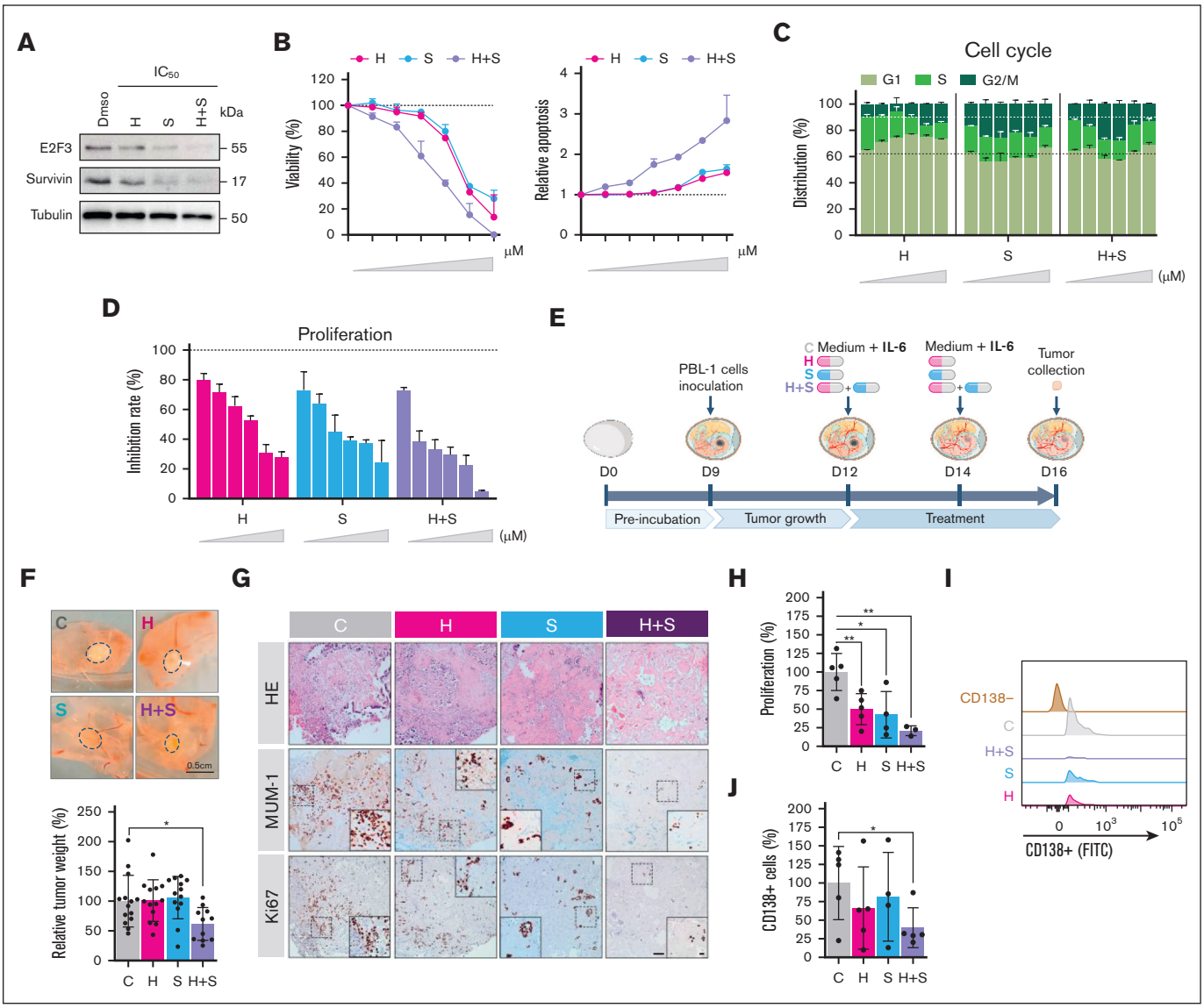


**Figure 6. E2F3 and survivin as possible therapeutic targets against PBL.** (A) Effect of H and S inhibitors, alone or in combination, in PBL-1 cells at $IC_{50}$ dose on E2F3 and survivin protein levels, as assessed by western blot. (B) The effect of the indicated inhibitors on viability and apoptosis was assessed by flow cytometry at 24 hours by annexin V/TO-PRO-3 staining in PBL-1 cells. Relative viability (%; left) and apoptosis (proportion; right) of treatments normalized to DMSO are shown. (C) Figure shows the distribution of cells in the cell cycle phases at 24 hours, which was evaluated by flow cytometry and TO-PRO-3 staining at different doses specified in the supplemental Materials and supplemental Table 2. (D) Effect of H, S, and H + S in cell proliferation measured by 3-(4,5-dimethylthiazol-2-yl)-2,5-diphenyltetrazolium bromide assay in PBL-1 cells. (E) Scheme followed to evaluate the effect of the H and S inhibitors alone and in combination in the chicken CAM based on the engraftment of PBL-1 cells on day 9, followed by 2 administrations of H, S, or H + S combination on days 12 and 14, and the collection of samples on day 16. (F) Tumors are weighted on day 16 (n = 7-14 eggs per group). Images of tumors under different conditions (top); and the relative reduction of tumor growth with the treatments (bottom). (G) Hematoxilin-eosin (HE), MUM-1, and Ki67 immunohistochemical (IHC) staining from sections of formalin-fixed, paraffin-embedded tumors from CAM under different treatment conditions (n = 5 eggs per group). (H) Relative proliferation of tumoral cells under different treatment conditions measured by Ki67 IHC staining. (I) The presence of $CD138^+$ cells in tumors formed without treatment or treated with H, S, or H+S assessed by CD138 (APC) staining and flow cytometry (n = 5 eggs per group). (J) The relative percentage of $CD138^+$ cells depending on the treatment of PBL-1 CAM model. All in vitro experiments were performed in biological triplicates. ANOVA test was used for statistical analysis. $^*P < .05$; $^{**}P < .01$; $^{***}P < .001$. C, control; DMSO, dimethyl sulfoxide; H, HLM006474; IL-6, interleukin-6; S, S12.

**Figure 5 (continued)** plus late) *E2F3*$^{mut}$ cells. (G) Gene expression (RT-qPCR) of miR-150-5p targets in WT vs *E2F3*$^{mut}$ transfected cells with NC or miR-150-p mimic. (H) Western blot plots of the protein expression of miR-150-5p targets in WT vs *E2F3*$^{mut}$ transfected cells with NC or miR-150-p mimic. (I) Relative protein expression of miR-150-5p targets. All experiments were performed in biological triplicates and technical duplicates, unless otherwise specified. Statistical significance was determined by *t* test. $^*P < .05$; $^{**}P < .01$; $^{***}P < .001$. GAPDH, glyceraldehyde-3-phosphate dehydrogenase; ns, not significant.

## Acknowledgments

The authors thank all patients and physicians for trial participation. MicroRNA expression studies were performed in the Microarrays Unit of the Josep Carreras Leukaemia Research Institute (Badalona, Spain); RNA sequencing was performed in the Centro Nacional de Análisis Genómico (Barcelona, Spain).

This study was supported by a grant from Instituto de Salud Carlos III, Ministerio de Economia y Competitividad (PI19/01588) and by the Josep Carreras Foundation, Spain.

## Authorship

Contribution: M.V.-B. designed the research, interpreted RNA sequencing and microarray data, performed and analyzed in vitro and in vivo studies, performed statistical analysis, and wrote the manuscript; M.J.B. acquired clinical data and extracted RNA of formalin-fixed, paraffin-embedded samples and designed the research; M.L.R. supported the preclinical design and supervised the study; A.M.L. performed bioinformatical analysis; M.E. contributed to bioinformatics studies; G.R. supported the preclinical design; N.P.-P. and M.P. performed in vivo studies; G.T., J.L.M., and I.A. performed the diagnostic review of samples; P.A., J.C., M.B.-O., J.M., M.A., E.G.-B., F.C., A.S., G.O., F.F., and G.L. provided plasmablastic lymphoma samples and clinical data of patients; J.-T.N. designed the research and supervised the study; and all authors read and approved the final manuscript.

Conflict-of-interest disclosure: J.-T.N. received research grants not related to this study from Gilead and EUSA Pharma/Recordati Rare Diseases, and honoraria not related to this study from AstraZeneca, Blueprint Medicines, EUSA Pharma/Recordati Rare Diseases, Novartis, and Roche. G.L. received research grants not related to this study from Agios, Aquinox, AstraZeneca, Bayer, Celgene, Gilead, Janssen, MorphoSys, Novartis, Roche, and Verastem, and honoraria not related to this study from ADC Therapeutics, AbbVie, Amgen, AstraZeneca, Bayer, BeiGene, Bristol Myers Squibb, Celgene, Constellation, Genase, Genmab, Gilead, Hexal/Sandoz, Immagene, Incyte, Janssen, Karyopharm, Lilly, Miltenyi, MorphoSys, Merck Sharp & Dohme, NanoString, Novartis, Pentixapharm, Pierre Fabre, Roche, and Sobi. G.R. reports research grants from Onconova Therapeutics. The remaining authors declare no competing financial interests.

The current affiliation for M.J.B. is Swedish Orphan Biovitrum, Stockholm, Sweden.

The current affiliation for M.L.R. is PharmaMar, Madrid, Spain.

ORCID profiles: M.V.-B., 0000-0003-4062-0549; M.J.B., 0000-0003-3471-2535; M.L.R., 0000-0003-4529-7832; A.M.-L., 0009-0002-0659-763X; M.P., 0009-0007-2801-7671; M.B.-O., 0000-0002-9431-4646; E.G.-B., 0000-0002-1323-1508; J.-M.S., 0000-0001-7168-6538; A.M.S., 0000-0002-5896-3200; I.A., 0000-0002-5043-6043; M.E., 0000-0003-4490-6093; G.T., 0000-0003-1882-0368; J.-T.N., 0000-0001-9101-6013.

Correspondence: José-Tomás Navarro, Josep Carreras Leukaemia Research Institute, Ctra de Can Ruti, Camí de les Escoles, s/n, 08916 Badalona, Spain; email: 2149684@uab.cat.

## References

1. Swerdlow SH, Campo E, Harris NL, et al. *WHO Classification of Tumours of Haematopoietic and Lymphoid Tissues*. 4th ed. International Agency for Research on Cancer (IARC); 2017.
2. Witte HM, Hertel N, Merz H, et al. Clinicopathological characteristics and MYC status determine treatment outcome in plasmablastic lymphoma: a multi-center study of 76 consecutive patients. *Blood Cancer J*. 2020;10(5):63.
3. Valera A, Balagué O, Colomo L, et al. IG/MYC rearrangements are the main cytogenetic alteration in plasmablastic lymphomas. *Am J Surg Pathol*. 2010;34(11):1686-1694.
4. Castillo JJ, Bibas M, Miranda RN. The biology and treatment of plasmablastic lymphoma. *Blood*. 2015;125(15):2323-2330.
5. Tchernonog E, Faurie P, Coppo P, et al. Clinical characteristics and prognostic factors of plasmablastic lymphoma patients: analysis of 135 patients from the LYSA group. *Ann Oncol*. 2017;28(4):843-848.
6. Frontzek F, Staiger AM, Zapukhlyak M, et al. Molecular and functional profiling identifies therapeutically targetable vulnerabilities in plasmablastic lymphoma. *Nat Commun*. 2021;12(1):5183.
7. Ramis-Zaldivar JE, Gonzalez-Farre B, Nicolae A, et al. MAP and JAK-STAT pathways dysregulation in plasmablastic lymphoma. *Haematologica*. 2021;106(10):2682-2693.
8. Witte HM, Künstner A, Hertel N, et al. Integrative genomic and transcriptomic analysis in plasmablastic lymphoma identifies disruption of key regulatory pathways. *Blood Adv*. 2022;6(2):637-651.
9. Liu Z, Filip I, Gomez K, et al. Genomic characterization of HIV-associated plasmablastic lymphoma identifies pervasive mutations in the JAK–STAT pathway. *Blood Cancer Discov*. 2020;1(1):112-125.
10. Ambrosio MR, Mundo L, Gazaneo S, et al. MicroRNAs sequencing unveils distinct molecular subgroups of plasmablastic lymphoma. *Oncotarget*. 2017;8(64):107356-107373.
11. Ameri A, Ahmed HM, Pecho RDC, et al. Diverse activity of miR-150 in tumor development: shedding light on the potential mechanisms. *Cancer Cell Int*. 2023;23(1):261.
12. Li F, Aljahdali I, Ling X. Cancer therapeutics using survivin BIRC5 as a target: what can we do after over two decades of study? *J Exp Clin Cancer Res*. 2019;38(1):368.
13. Kent LN, Leone G. The broken cycle: E2F dysfunction in cancer. *Nat Rev Cancer*. 2019;19(6):326-338.

14. Chen H-Z, Tsai S-Y, Leone G. Emerging roles of E2Fs in cancer: an exit from cell cycle control. *Nat Rev Cancer*. 2009;9(11):785-797.
15. Li Y, Choi PS, Casey SC, Dill DL, Felsher DW. MYC through miR-17-92 suppresses specific target genes to maintain survival, autonomous proliferation, and a neoplastic state. *Cancer Cell*. 2014;26(2):262-272.
16. Mihailovich M, Bremang M, Spadotto V, et al. miR-17-92 fine-tunes MYC expression and function to ensure optimal B cell lymphoma growth. *Nat Commun*. 2015;6(1):8725.
17. Jiang X, Huang H, Li Z, et al. Blockade of miR-150 maturation by MLL-fusion/MYC/LIN-28 is required for MLL-associated leukemia. *Cancer cell*. 2012; 22(4):524-535.
18. Tung C-H, Kuo L-W, Huang M-F, et al. MicroRNA-150-5p promotes cell motility by inhibiting c-Myb-mediated Slug suppression and is a prognostic biomarker for recurrent ovarian cancer. *Oncogene*. 2020;39(4):862-876.
19. Liu Z, Wang P, Yuan S, et al. LncRNA BC200/miR-150-5p/MYB positive feedback loop promotes the malignant proliferation of myelodysplastic syndrome. *Cell Death Dis*. 2022;13(2):126.
20. Nakata Y, Shetzline S, Sakashita C, et al. c-Myb plays a role in G2/M cell cycle transition by direct regulation of cyclin B1 expression. *Cancer Res*. 2005; 65(suppl 9):1278.
21. Chapman J, Gentles AJ, Sujoy V, et al. Gene expression analysis of plasmablastic lymphoma identifies downregulation of B-cell receptor signaling and additional unique transcriptional programs. *Leukemia*. 2015;29(11):2270-2273.
22. Meng X, Deng Y, He S, Niu L, Zhu H. m6A-mediated upregulation of LINC00857 promotes pancreatic cancer tumorigenesis by regulating the miR-150-5p/E2F3 Axis. *Front Oncol*. 2021;11:629947.
23. Jiang Y, Saavedra HI, Holloway MP, Leone G, Altura RA. Aberrant regulation of survivin by the RB/E2F family of proteins. *J Biol Chem*. 2004;279(39): 40511-40520.
24. Carmena M, Wheelock M, Funabiki H, Earnshaw WC. The chromosomal passenger complex (CPC): from easy rider to the godfather of mitosis. *Nat Rev Mol Cell Biol*. 2012;13(12):789-803.
25. Musilova K, Devan J, Cerna K, et al. miR-150 downregulation contributes to the high-grade transformation of follicular lymphoma by upregulating FOXP1 levels. *Blood*. 2018;132(22):2389-2400.
26. Xie D, Pei Q, Li J, Wan X, Ye T. Emerging role of E2F family in cancer stem cells. *Front Oncol*. 2021;11:11723137.
27. Wu L, Wan S, Li J, et al. Expression and prognostic value of E2F3 transcription factor in non-small cell lung cancer. *Oncol Lett*. 2021;21(5):411.
28. Feng Z, Peng C, Li D, et al. E2F3 promotes cancer growth and is overexpressed through copy number variation in human melanoma. *Onco Targets Ther*. 2018;11:5303-5313.
29. Zhang L, Yao Y, Zhang S, et al. Metabolic reprogramming toward oxidative phosphorylation identifies a therapeutic target for mantle cell lymphoma. *Sci Transl Med*. 2019;11(491):eaau1167.
30. Guièze R, Liu VM, Rosebrock D, et al. Mitochondrial reprogramming underlies resistance to BCL-2 inhibition in lymphoid malignancies. *Cancer Cell*. 2019;36(4):369-384.e13.
31. Ohi N, Okuno M, Tanaka H, Ohtani T. Combination therapy strategy for lymphoma based on cancer energy metabolism of OPB-111077, a novel antitumor agent inhibiting mitochondrial oxidative phosphorylation. *Blood*. 2021;138(suppl 1):4363.
32. Noble RA, Thomas H, Zhao Y, et al. Simultaneous targeting of glycolysis and oxidative phosphorylation as a therapeutic strategy to treat diffuse large B-cell lymphoma. *Br J Cancer*. 2022;127(5):937-947.
33. Dolcetti R, Gloghini A, Caruso A, Carbone A. A lymphomagenic role for HIV beyond immune suppression? *Blood*. 2016;127(11):1403-1409.
34. Laurent C, Fabiani B, Do C, et al. Immune-checkpoint expression in Epstein-Barr virus positive and negative plasmablastic lymphoma: a clinical and pathological study in 82 patients. *Haematologica*. 2016;101(8):976-984.
35. Verdu-Bou M, Tapia G, Hernandez-Rodriguez A, Navarro J-T. Clinical and therapeutic implications of Epstein–Barr virus in HIV-related lymphomas. *Cancers (Basel)*. 2021;13(21):5534.
36. Liu F, Di Wang X. miR-150-5p represses TP53 tumor suppressor gene to promote proliferation of colon adenocarcinoma. *Sci Rep*. 2019;9(1):6740.
37. Sugita BM, Rodriguez Y, Fonseca AS, et al. MiR-150-5p overexpression in triple-negative breast cancer contributes to the in vitro aggressiveness of this breast cancer subtype. *Cancers (Basel)*. 2022;14(9):2156.
38. Suetsugu T, Koshizuka K, Seki N, et al. Downregulation of matrix metalloproteinase 14 by the antitumor miRNA, miR-150-5p, inhibits the aggressiveness of lung squamous cell carcinoma cells. *Int J Oncol*. 2018;52(3):913-924.
39. Mizuno K, Tanigawa K, Misono S, et al. Regulation of oncogenic targets by tumor-suppressive *miR-150-3p* in lung squamous cell carcinoma. *Biomedicines*. 2021;9(12):1883.
40. Peng Y, Croce CM. The role of MicroRNAs in human cancer. *Sig Transduct Target Ther*. 2016;1(1):15004.
41. Robaina MC, Mazzoccoli L, Klumb CE. Germinal centre B cell functions and lymphomagenesis: circuits involving MYC and MicroRNAs. *Cells*. 2019; 8(11):1365.
42. Wang X, Zhao X, Gao P, Wu M. c-Myc modulates microRNA processing via the transcriptional regulation of Drosha. *Sci Rep*. 2013;3(1):1942.
43. Tao J, Zhao X, Tao J. c-MYC–miRNA circuitry: a central regulator of aggressive B-cell malignancies. *Cell Cycle*. 2014;13(2):191-198.

44. Singh A, Spitzer MH, Joy JP, et al. Postmitotic G1 phase survivin drives mitogen-independent cell division of B lymphocytes. *Proc Natl Acad Sci U S A*. 2022;119(18):e2115567119.
45. Song J, Salek-Ardakani S, So T, Croft M. The kinases aurora B and mTOR regulate the G1-S cell cycle progression of T lymphocytes. *Nat Immunol*. 2007;8(1):64-73.
46. Kong L-J, Chang JT, Bild AH, Nevins JR. Compensation and specificity of function within the E2F family. *Oncogene*. 2007;26(3):321-327.
47. Xu L, Yu W, Xiao H, Lin K. BIRC5 is a prognostic biomarker associated with tumor immune cell infiltration. *Sci Rep*. 2021;11(1):390.
48. Fäldt Beding A, Larsson P, Helou K, Einbeigi Z, Parris TZ. Pan-cancer analysis identifies BIRC5 as a prognostic biomarker. *BMC Cancer*. 2022;22(1):322.
49. Lan W, Bian B, Xia Y, et al. E2F signature is predictive for the pancreatic adenocarcinoma clinical outcome and sensitivity to E2F inhibitors, but not for the response to cytotoxic-based treatments. *Sci Rep*. 2018;8(1):8330.
50. Brun SN, Markant SL, Esparza LA, et al. Survivin as a therapeutic target in Sonic hedgehog-driven medulloblastoma. *Oncogene*. 2015;34(29):3770-3779.
51. Albadari N, Li W. Survivin small molecules inhibitors: recent advances and challenges. *Molecules*. 2023;28(3):1376.
52. Ma Y, Kurtyka CA, Boyapalle S, et al. A small-molecule E2F inhibitor blocks growth in a melanoma culture model. *Cancer Res*. 2008;68(15):6292-6299.
53. Kurtyka CA, Chen L, Cress WD. E2F inhibition synergizes with paclitaxel in lung cancer cell lines. *PLOS ONE*. 2014;9(5):e96357.